# Nanoscale carrier multiplication mapping in a Si diode

Corentin Durand, Pierre Capiod, Maxime Berthe, Jean-Philippe Nys, Christophe Krzeminski, Didier Stiévenard, Christophe Delerue, B. Grandidier

# Nanoscale carrier multiplication mapping in a Si diode

Corentin Durand,[†] Pierre Capiod, Maxime Berthe, Jean Philippe Nys, Christophe Krzeminski, Didier Stiévenard, Christophe Delerue, Bruno Grandidier [*]

*Institut d'Electronique, de Microélectronique et de Nanotechnologies (IEMN), CNRS, UMR 8520*

*Département ISEN, 41 bd Vauban, 59046 Lille Cedex, France*

[†] Present address : Center for Nanophase Materials Sciences, Oak Ridge National Laboratory, Oak Ridge, Tennessee 37831-6487, USA

[*] B. Grandidier. E-mail: bruno.grandidier@isen.iemn.univ-lille1.fr

ABSTRACT

Carrier multiplication (CM), the creation of electron-hole pairs from an excited electron, has been investigated in a silicon *p-n* junction by multiple probe scanning tunneling microscopy. The technique enables an unambiguous determination of the quantum yield based on the direct measurement of both electron and hole currents, that are generated by hot tunneling electrons. The combined effect of impact ionization, carrier diffusion and recombination is directly visualized from the spatial mapping of the CM efficiency. Atomically well-ordered areas of the *p-n* junction surface sustain the highest CM rate, demonstrating the key role of the surface in reaching high yield.

Keywords: Carrier multiplication, impact ionization, silicon, multiple probe scanning tunneling microscopy

Under illumination, charge carriers in semiconductor materials gain an energy that can far exceed the semiconductor bandgap. To return to the equilibrium conditions, several relaxation mechanisms exist. The predominant one in bulk materials corresponds to a transfer of energy to the lattice through phonon emission. But hot carriers can also scatter with other charge carriers leading to impact ionization phenomena. The generation of new electron-hole pairs, that supplants the energy transfer through heat dissipation, is very attractive for power conversion and photodetection applications. Strong efforts are devoted to increase its efficiency through the design of novel nanomaterials or clever band structure engineering.[1,2,3] For example, intensive work has been achieved to study carrier multiplication (CM) in semiconductor nanoscrystals,[4,5] with the hope to improve the efficiency of solar cell.[6,7] Recently, high CM rates have also been demonstrated in avalanche photodiodes and phototransistors based on the use of semiconductor heterostructure nanowires and hybrid graphene-quantum dot systems.[8,9]

Hot carriers are usually generated by the absorption of photons with sufficient excess energy above the band gap. The dynamics of photogenerated carriers as well as the carrier population have been successfully probed with time-resolved optical spectroscopic techniques. [4,5] But, in these experiments, the relaxation of electron and holes can not be distinguished, the generated charge carriers are not collected as a photocurrent, and, due to the limited spatial resolution of the photon source, the experiments involve the integration of data over a volume many times the size of nanomaterials such as quantum dots. Therefore, the demonstration of a photocurrent resulting from CM is an important research goal and should take along with an increase of the spatial resolution. To solve this issue, scanning tunneling microscopy is quite appropriate since this technique produces a spatially localized beam of electrons with variable energy. When it is used to perform ballistic electron emission microscopy (BEEM), it has been shown that a fraction of the collected current consists of electrons generated by hot incident electrons.[10] However, separating their contributions from the ballistic electrons to determine the quantum yield (QY) for CM is not straightforward and might be fraught with incertainty (see Supporting Information).

A more accurate approach for measuring QY would consist in collecting not only the generated electrons, but also the excited holes, since CM implies the creation of electron-hole pairs. Indeed, their detection constitutes the most compelling evidence for the production of extra charge carriers. In this work, we report a novel method to measure QY in materials and devices that fulfils both requirements: a localized excitation of the hot electrons and a detection setup that measures the generated electron and hole currents, enabling the direct mapping of QY at the nanoscale. The experimental scheme, that is based on the use of a multiple probe scanning tunneling microscopy (STM) system,[11,12,13] is depicted in Figure 1a. Two STM tips in electrical contact with the highly doped regions of a *p*-*n* junction polarizes the diode in reverse-bias. A third tip injects tunneling electrons into the conduction band states of the sample at a well defined energy (current $I_t$). At small energy separation between the Fermi level of this tip and the bottom of the conduction band in the sample, the tunneling electrons drift through the *n* layer, as shown in the upper energy band diagram of Figure 1a. When the energy separation exceeds the carrier multiplication threshold (lower energy diagram), the tunneling electrons generate electron-hole pairs. The tunneling electrons and the generated electrons (current $I_{e^-}$) flow towards the $n^{++}$ contact, whereas holes (current $I_{h^+}$) flow towards the $p^{++}$ contact and are readily measured. The comparison between the increase of the hole and electron currents and the tunneling current allows to unambiguously quantify the product of CM with the collection efficiency in the diode. Furthermore, as the tunneling tip can be scanned over the whole surface of the sample, measurements of the different currents yield the minority carrier diffusion length outside the space charge layer and a spatial map of QY in the space charge layer, due to the efficient separation of the charge carriers in this region.

To achieve this goal, we built Si diodes in a *n*-type (100) silicon wafer doped with $4.5 \times 10^{16}$ $As.cm^{-3}$. The scanning electron microscopy (SEM) image of a typical Si diode is shown in Figure 1b. The $p^{++}$ and $n^{++}$ regions are clearly identified, the $p^{++}$ region exhibiting a brighter contrast, relative to the *n*-type regions, consistent with the literature.[14] By contacting both highly doped regions with tips 1 and 2 in ultra high vacuum (UHV), a good rectifying behaviour is measured (Figure 1c). Based on the

simulation of the dopant profile in the diode (Figure 1d), we estimate the width $x_n=\sqrt{(2\varepsilon_r V_{bi}/eN_D)}$ of the space charge layer to be in the range of 150 nm, where $\varepsilon_r$ is the dielectric constant of silicon, $V_{bi}$ the built-in potential, $e$ the elementary charge and $N_D$ the donor concentration of the substrate. With the help of the SEM image, tip 3 is then positioned in tunneling regime above the space charge layer. Spectroscopic measurements are performed with a closed feedback loop.[15] In this regime, the tunneling current is kept constant, whatever the bias $V_t$ applied between the $n^{++}$ region and tip 3, as seen in Figure 2(a). Along with the measurement of the tunneling current that is injected by tip 3, the current due to the majority carriers in the *n* and *p* regions are also measured with tips 1 and 2, the diode being slightly reverse biased with a voltage $V_p$ of -15mV. We note that the sum of all three currents should be zero with the reference direction of the currents chosen in Figure 1(a).

Figure 2(b) shows a set of spectra for the electron current $I_{e-}$ measured with tip 1 at the different setpoint currents $I_t$. Below $V_t$=2V, the difference between the electron current $I_{e-}$ and the polarization current of 64 pA, that is caused by the reverse bias of the diode, is strictly opposite to the tunneling current $I_t$. In this voltage range, a small hole current $I_{h+}$ is also measured and corresponds to the polarization current of the diode (see Figure 2(c) and Figure S2(d) in the Supporting Information). We note that $I_{h+}$ and $I_{e-}$ have opposite signs, because tip 2 and tip 1 collect holes and electrons respectively. Above $V_t$=2V, $I_{h+}$ and $I_{e-}$ first slightly varies and, then, when $V_t$ becomes higher than 4V, strongly increases, whereas $I_t$ is maintained constant. This observation is verified whatever the setpoint current, meaning that additional charge carriers are generated in the junction. The number of electrons and holes respectively collected by tips 2 and 3 are roughly symmetric. We thus attribute this increase to impact ionization, where a hot tunneling electron relax to the conduction band edge by generating an electron-hole pair.

QY is usually defined as the number of created electron-hole pairs divided by the number of injected electrons. We stress that generated electrons and holes can be lost, because of the (surface) recombination processes that take place during the time the carriers diffuse or drift in the diode. As a

result, the measured QY corresponds to the net extra-charge carriers, that are effectively collected by tips 1 and 2, divided by the number of injected electrons:

$$QY = \frac{(I_{h+} - I_{pol}) + (-I_{e-} - I_t - I_{pol})}{2I_t} \quad (1)$$

QY is plotted in Figure 2d. It rises rapidly above $V_t$=4V, reaches a plateau and then increases almost linearly, consistent with theoretical predictions of impact ionization in Si[16] and BEEM experiments.[10] However, we note small variations between our result and these previous works. The first one is related to the threshold voltage, for which impact ionization starts. It depends on the energy onset of impact ionization and the position of the conduction band states relative to the Fermi level. In our case, the Fermi level is pinned at the bottom of the $\pi^*$ surface states band, 0.85 eV above the top of the valence band.[17] Because the screening of the electric field by the surface states is only partial on the Si(100) surface, a stronger tip-induced band bending arises in comparison with Ref. 10, accounting for a higher threshold voltage. We also see a dip in the current $I_{h+}$ between $V_t$=2V and 4V. We suggest that it is caused by the upward tip-induced band bending in the depletion layer (see section 3 of the Supporting Information), favoring the drift of electrons towards the $p^{++}$ region and making the current $I_{h+}$ negative. Finally, the generation of electron-hole pairs corresponding to the plateau ($V_t$=6V) is smaller than the one predicted in Ref. 16 for reasons discussed below.

In order to grab the influence of the surface on the lifetime of the generated charge carriers, we have first studied the currents $I_{e-}$ and $I_{h+}$ as a function of the lateral position of tip 3 at a voltage higher than the threshold voltage. For that purpose, the feedback of the STM adjusts the distance between tip 3 and the Si(100) surface at constant $V_t$, while tip 3 is scanning and the diode reverse biased. Figure 3a highlights an area of the Si(100) surface, defined by the yellow dotted rectangle, where the topography and the map related to $I_{h+}$ have been simultaneously acquired at $V_t$=7V (insets of Figure 3a and b respectively). The clusters seen at the right of the topography corresponds to the defective inner corolla region at the boundary of the $n^{++}$ region. The corrugation of the outer corolla looks smoother in the

topography consistent with the SEM image (700 nm < x < 1000nm). Further away the roughness increases, but no significant change is visible between the lightly doped *n*-type region and the $p^{++}$ region. Only the overall colour contrast becomes slightly brighter in the left part of the image, suggesting a modification of the electrical property of the layer. The image of the $I_{h+}$ signal (inset of Figure 3b) shows much stronger contrast variations that are assigned, based on the SEM image of Figure 3a from right to left, to the $n^{++}$ region (dark), the lightly doped *n* region, the space charge layer (very bright) and the $p^{++}$ region (black).

A better resolved variation of $I_{h+}$ is also seen in the line profile of Figure 3b, when tip 3 scans the surface in line mode. In the lightly doped *n* region close to the $n^{++}$ region, the intensity of $I_{h+}$ is primarily given by $I_{pol}$, because the holes generated by impact ionization rapidly recombine with the majority charge carriers. As tip 3 moves towards the $p^{++}$ region, more and more holes reach the space charge layer and are extracted by the built-in electric field to be collected by tip 2. In the space charge layer that shows a width of 80 nm, slightly smaller than the estimated width, the signal saturates: electrons and holes are efficiently separated and collected by the electrodes. Finally, in the $p^{++}$ region, the negative signal indicates that the electrons are now collected by tip 2.

A comprehensive analysis of the charge carrier dynamics is achieved by analytically solving the continuity equation using an one-dimensional model. In steady state, the continuity equation for holes in the *n*-type region is given by:

$$D_p \frac{\partial^2 p(x)}{\partial x^2} - \mu_p \xi \frac{\partial p(x)}{\partial x} + \gamma \delta (x - x_g) - \frac{p(x)}{\tau_p} = 0 \qquad (2)$$

where $p$, $D_p$, $\mu_p$, $\gamma$ and $\tau_p$ are the hole concentration, the hole diffusion coefficient, the hole mobility, the hole generation rate and the carrier lifetime. In this equation, the first and second terms correspond to the diffusion and the drift of holes that are respectively driven by the hole density gradient and the electric field $\xi$. The third term is the generation of holes from impact ionization. It solely occurs at the position of tip 3, labelled $x_g$ in Figure 1a, and is thus modeled with a delta function δ. The last term corresponds

to the recombination of holes in bulk and at the surface. The equation can be solved using the Laplace transform, by fulfilling two boundary conditions: (i) all holes are extracted by the built-in electric field once they have reached the depletion region, consistent with the experimental saturation of the hole current in this region, meaning $p(x_n)=0$; (ii) the hole current density at the place of generation equals $\gamma e$. Calculations of the current density at the position $x_n$ as a function of $x_g$ allows to fit the current profile of Figure 3b by adjusting $\tau_p$.

From the curve fitting, we deduce a hole carrier diffusion length of $L_p = \sqrt{\tau_p D_p}$ =80 nm in the lightly doped *n*-type region. This value is much smaller than the expected diffusion length in bulk for the related dopant concentration.[18] Although a more accurate analysis should have taken into account the modification of the surface potential induced by tip 3, this large discrepancy reveals a fast recombination of the holes with a lifetime of $\tau_p \approx 6.4$ps. Ignoring the negligible contribution of the bulk carrier lifetime, $\tau_p$ is given by the ratio between the width of the hole accumulation layer, caused by the surface pinning of the Fermi level above midgap, and the surface recombination velocity *S*.[19] With the width deduced from the surface built-in potential of 100 meV in the lightly doped *n*-type region, *S* is found to be three orders of magnitude higher than the surface recombination velocity measured on an atomically well-ordered Si(100) surface.[20] While the low energy electron diffraction (LEED) pattern of the sample surface is consistent with the typical (2x1) reconstruction (Figure 3c), the STM images do not only reveal the presence of Si dimer rows (Figure 3d), but also many point defects and clusters, in agreement with the SEM image. Based on the analysis of the surface composition with Auger spectroscopy (Figure 3e), the presence of carbon and oxygen peaks prior to the UHV sample preparation suggest that the observed clusters are primarily made up of silicon and silicon carbide after annealing at a temperature of 850°C. All these surface defects trap the diffusing holes and account for a high surface recombination velocity.[21]

The loss of generated carriers is directly visible in the quantum yield image that is calculated with equation (1) and shown in Figure 4b at $V_t$ =7V. In the lightly doped n-type region (right part of this image), QY is always below 0.5 and rapidly decreases to zero as tip 3 moves away from the space charge layer, consistent with a higher number of clusters on the way of the charge carriers. Conversely, in the space charge layer, QY approaches one, indicating that the generated charge carriers drift without being trapped by the clusters. This is particularly true in atomically flat areas that are separated by clusters from the $p^{++}$ region (Figure 4a). They show a similar QY as the clean areas that appear bright all along the width of the space charge layer.

Interestingly, the comparison of the topography and the QY image in the space charge layer shows that QY is always smaller when tip 3 injects electrons on the clusters. While this effect could be caused by a higher threshold voltage due to a difference of work function between the clean areas and the clusters, Figure 4c readily shows that this is not the case. For the majority of clusters, the threshold voltage was not found to significantly change. Therefore, the reduction of QY in the clusters is either caused by a reduction of the density of states in comparison with the bulk state of Si,[2,22] or by ineslastic scattering of electrons and/or by a fast recombination of the generated electron and hole. This last explanation is in line with surface photovoltage measurements that found a recombination rate four times higher on similar clusters than on Si dangling bonds on the Si(111)-(7x7) surface.[23] It is consistent with the short lifetimes between 1 and 100ps that have been predicted in semiconductor nanocrystals due to multiphonon capture by localized surface states.[24] It could also involve, albeit to a much lesser extent, the radiative recombination of the generated holes with additional hot electrons supplied by tip 3, giving rise to ultraviolet luminescence.[25,26]

In conclusion, we have described a new method to study CM in semiconductor junctions. As the technique discriminates between charge carriers of opposite sign, it provides a direct and accurate determination of QY. Its use offers several benefits, a high spatial resolution, a strong sensitivity to trapping centers at the surface, an arbitrary arrangements of the probe. Because the tunneling electrons

can also be transferred through thin oxide layers and have a penetration of a few nanometers in the semiconductor materials, we envision that the same technique is suitable in air or in liquid using either a STM tip or the probe of a conductive atomic force microscope. This technique being quite versatile, it opens up interesting prospects for the investigation of CM efficiency in more complex semiconductor materials at the nanoscale as well as the study of avalanche amplification in electronic and optoelectronic devices.

## REFERENCES


1. Gabor, N. M.; Zhong, Z.; Bosnick, K.; Park, J.; McEuen, P. L. *Science* **2009**, *325*, 1367-1371.
2. Pijpers, J. J. H.; Ulbricht, R.; Tielrooj, K. J., Osherov, A.; Golan, Y.; Delerue, C.; Allan, G.; Bonn, M. *Nat. Phys.* **2009**, ***5***, 811-814.
3. Winzer, T.; Knorr, A.; Malic, E. *Nano Lett.* **2010**, *10*, 4839-4843.
4. Schaller, R. D.; Klimov, V. *Phys. Rev. Lett.* **2004**, *92*, 186601.
5. Trinh, M. T.; Houtepen, A. J.; Schins, J. M.; Hanrath, T.; Piris, J.; Knulst, W.; Siebbeles, L. D. A. *Nano Lett.* **2008**, *8*, 1713-1718.
6. Sukhovatkin, V.; Hinds, S.; Brzozowski, L.; Sargent, E. H. *Science* **2009**, *324*, 1542-1544.
7. Semonin, O. E.; Luther, J. M.; Choi, S.; Chen, H.-Y.; Gao, J.; Nozik, A. J.; Beard M. C. *Science* **2011**, *334*, 1530-1533.
8. Bulgarini, G.; Reimer, M. E.; Hocevar, M.; Bakkers, E. P. A M.; Kouwenhoven, L. P.; Zwiller, V. *Nat. Photonics* **2012**, *6*, 455-458.
9. Konstantatos, G.; Badioli, M.; Gaudreau, L.; Osmond, J.; Bernechea, M.; Garcia de Arquer, P. F.; Gatti, F.; Koppens, F. H. L. *Nat. Nanotech.* **2012**, *7*, 363-368.
10. Bauer, A.; Ludeke, R. *Phys. Rev. Lett.* **1994**, *72*, 928-931.
11. Shiraki, I.; Tanabe, F.; Hobara, R.; Nagao, T.; Hasegawa, S. *Surf. Sci.* **2001**, *493*, 633-643.
12. Kim, T. H.; *et al*., *Nano Lett.* **2010**, *10*, 3096-3100.
13. Durand, C.; Berthe, M.; Makoudi, Y.; Nys, J.-P.; Leturcq, R.; Caroff, P.; Grandidier, B. *Nanotechnology* **2013**, *24*, 275706.
14. Elliott, S. L.; Broom, R. F.; Humphreys, C. J. *J. Appl. Phys.* **2002**, *91*, 9116-9122.
15. Nguyen, T. H.; Mahieu, G.; Berthe, M.; Grandidier, B.; Delerue, C.; Stiévenard, D.; Ebert, Ph. *Phys. Rev. Lett.* **2010**, *105*, 226404.
16. Alig, R. C.; Bloom, S.; Struck, C. W. *Phys. Rev. B* **1980**, *22*, 5565-5582.

17. Dubois, M.; Perdigão, L.; Delerue, C.; Allan, G.; Grandidier, B.; Deresmes, D.; Stiévenard, D. *Phys. Rev. B* **2005**, *71*, 165322.
18. Del Alamo, J. A.; Swanson, R. M. *Solid-State Electron.* **1987**, *30*, 1127-1136.
19. Yablonovitch, E.; Allara, D. L.; Chang, C. C.; Gmitter, T.; Bright, T. B. *Phys. Rev. Lett.* **1986**, *57*, 249-252.
20. Weinelt, M.; Kutschera, M.; Fauster, T.; Rohlfing, M. *Phys. Rev. Lett.* **2004**, *92*, 126801.
21. Sabbah, A. J.; Riffe, D. M. *J. Appl. Phys.* **2000**, *88*, 6954.
22. Allan, G.; Delerue, C. *ACS Nano* **2011**, ***5***, 7318-7323.
23. Hamers, R. J.; Market, K. *Phys. Rev. Lett.* **1990**, *64*, 1051-1054.
24. Allan, G.; Delerue, C. *Phys. Rev. B* **2012**, *79*, 195324.
25. Schmidt, P.; Berndt, R. *Phys. Rev. Lett.* **2007**, *99*, 246103.
26. De Boer, W. D. A. M.; Timmerman, D.; Dohnalova, K.; Yassievich, I. N.; Zhang, H.; Buma, W. J.; Gregorkiewicz, T. *Nat. Nanotech.* **2010**, *5*, 878-884.

## ASSOCIATED CONTENT

### Supporting information

Materials and methods, comparison of BEEM/multiple probe STM, tunneling tip influence on the experiments. This material is available free of charge via the Internet at http://pubs.acs.org.

## ACKNOWLEDGMENTS

This study was financially supported by the EQUIPEX program Excelsior, the french RENATECH network and the European Community's Seventh Framework Program (Grant No. PITN-GA-2012-316751, "Nanoembrace" project). C. Durand acknowledges the financial support of the DGA. We thank Y. Coffinier for technical assistance.

FIGURES

**Figure 1**. (a) Experimental scheme for the measurement of the carrier multiplication rate in a Si diode. Two STM tips 1 and 2 are in contact with the $n^{++}$ and $p^{++}$ regions of a diode that is polarized with a reverse bias $V_p$. The third STM tip injects tunneling electrons to the Si(100) surface at a bias $V_t$. At low bias, the electrons relax to the bottom of the conduction band (CB) and diffuse towards the $n^{++}$ region, where they are collected as a current $I_{e-}$. At high bias, the relaxation of the electron leads to the generation of an electron-hole pair. Both electrons diffuse towards the $n^{++}$ region, while the hole in the valence band (VB) drifts towards the $p^{++}$ region, where it is collected as a current $I_{h+}$ by tip 2. (b) Scanning electron micrograph of the Si diode, where the highly doped regions are respectively labelled $p^{++}$ and $n^{++}$, the lateral extent of the space charge region being delimited by the curved dotted lines at the positions $x = 0$ and $x_n$ respectively. (c) Diode electrical characteristic. (d) Simulated dopant profile across the junction. Positive and negative values correspond to donor and acceptor concentrations respectively.

**Figure 2.** Simultaneous measurement in closed loop of (a) tunneling current spectra, (b) electron current ($I_{e-}$) spectra and (c) hole current ($I_{h+}$) spectra acquired with tips 3, 1 and 2 respectively. The measurement was performed in the space charge layer. (d) Voltage dependence of the quantum yield. For clarity, the plots of the quantum yield are restricted to six different setpoints for the tunneling current.

**Figure 3.** (a) Scanning electron micrograph of a Si diode, where the area scanned with tip 3 is delimited by the dotted rectangle. Inset: STM image acquired in the dotted rectangle ($V_t$=7V, $I_t$=1nA, scan rate: 0.036 Hz). (b) Hole current profile averaged 30 times when scanning a single line across the junction. The red line shows the calculated fit of the hole current based on the continuity equation. Inset: Hole

current image acquired simultaneously with the topography shown in the inset of (a). (c) LEED pattern of the sample surface showing the (2x1) structure of the Si(100) surface. (d) High resolution STM image of the sample surface ($V_t$=-2V, $I_t$=0.1nA). (e) Auger electron spectroscopy spectrum of the sample surface prior to the Joule heating. C and O yield for carbon and oxygen species respectively.

**Figure 4**. Simultaneously acquired (a) topography and (b) map of the carrier multiplication efficiency in the vicinity of the space charge layer (SCL) of the p-n junction ($V_t$=7V, $I_t$=1nA, scan rate: 0.036 Hz). (c) Voltage dependence of the quantum yield measured on a clean area (black) and on a cluster (red).

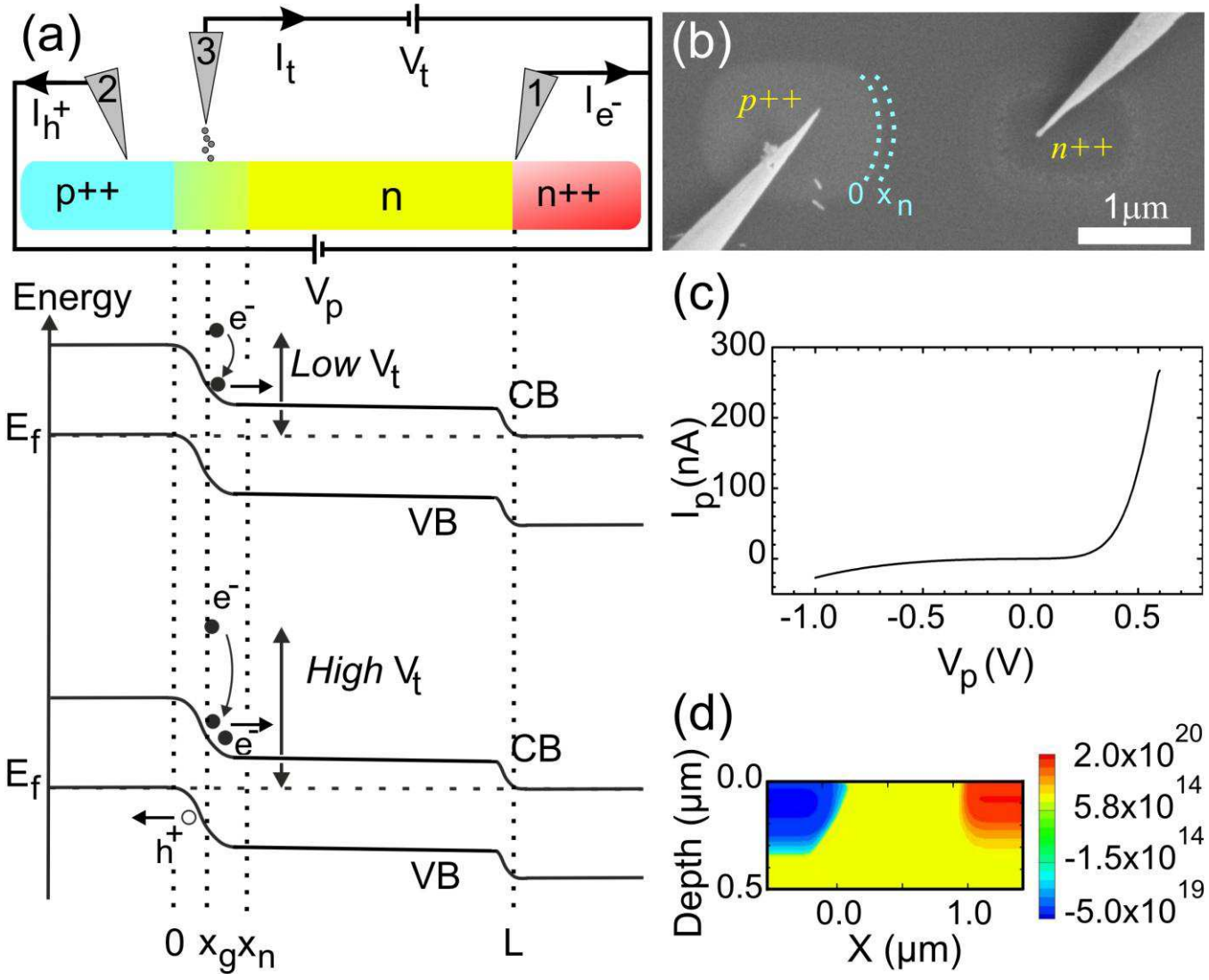
(a)
3
$I_t$
$V_t$
2
$I_h^+$
1
$I_e^-$
p++
n
n++
$V_p$
Energy
$e^-$
Low $V_t$
CB
$E_f$
VB
$e^-$
High $V_t$
$e^-$
CB
$E_f$
$h^+$
VB
0 $x_g$ $x_n$
L
(b)
p++
n++
0 $x_n$
1μm
(c)
300
200
100
0
$I_p$(nA)
-1.0
-0.5
0.0
0.5
$V_p$ (V)
(d)
Depth (μm)
0.0
0.5
0.0
1.0
X (μm)
$2.0x10^{20}$
$5.8x10^{14}$
$-1.5x10^{14}$
$-5.0x10^{19}$

FIGURE 1

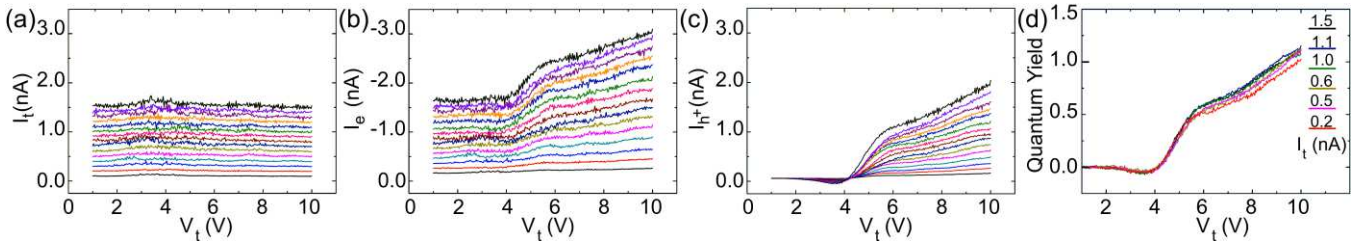
(a)
$I_t$(nA)
$V_t$ (V)
(b)
$I_e$ (nA)
$V_t$ (V)
(c)
$I_h$+(nA)
$V_t$ (V)
(d)
Quantum Yield
$V_t$ (V)
1.5
1.1
1.0
0.6
0.5
0.2
$I_t$ (nA)

FIGURE 2

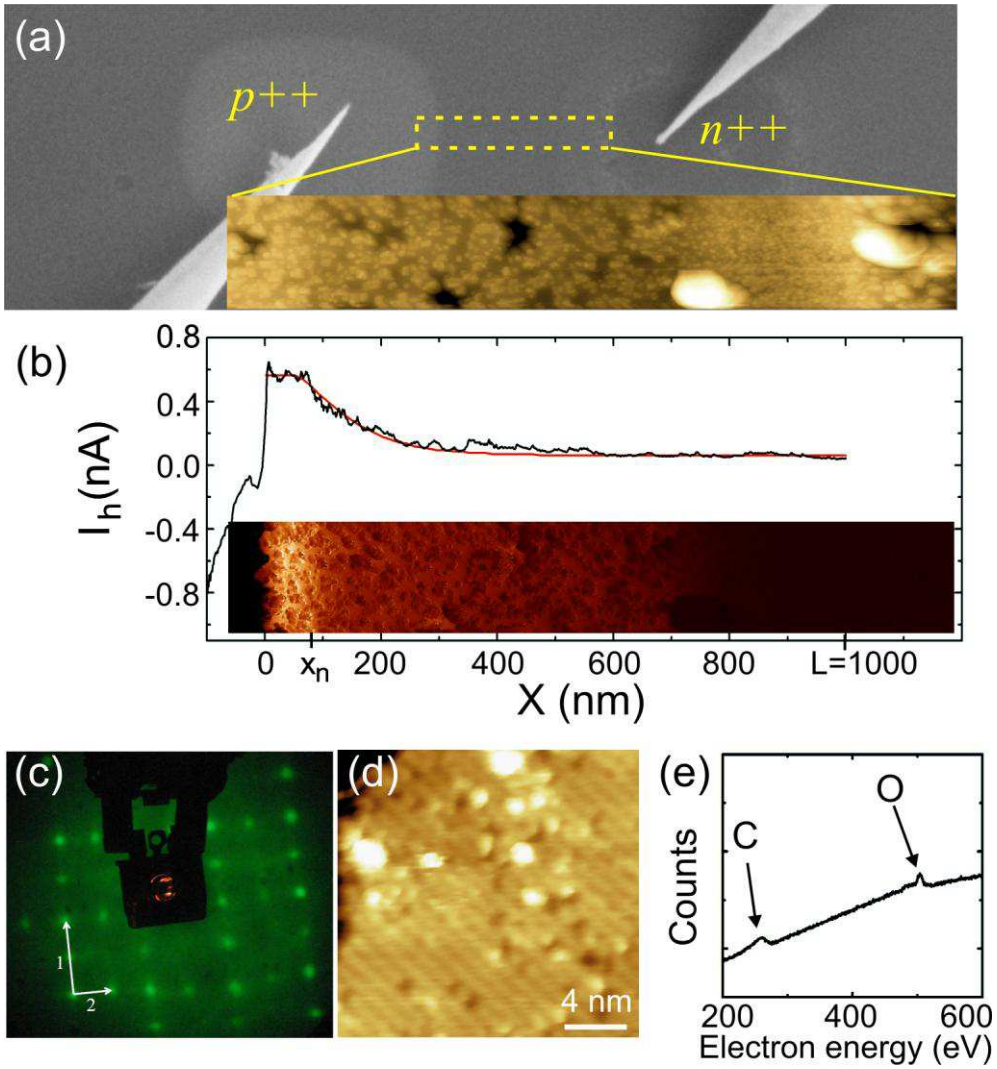
(a)
p++
n++
(b)
0.8
0.4
0.0
-0.4
-0.8
I_h(nA)
0
x_n
200
400
600
800
L=1000
X (nm)
(c)
1
2
(d)
4 nm
(e)
O
C
Counts
200
400
600
Electron energy (eV)

FIGURE 3

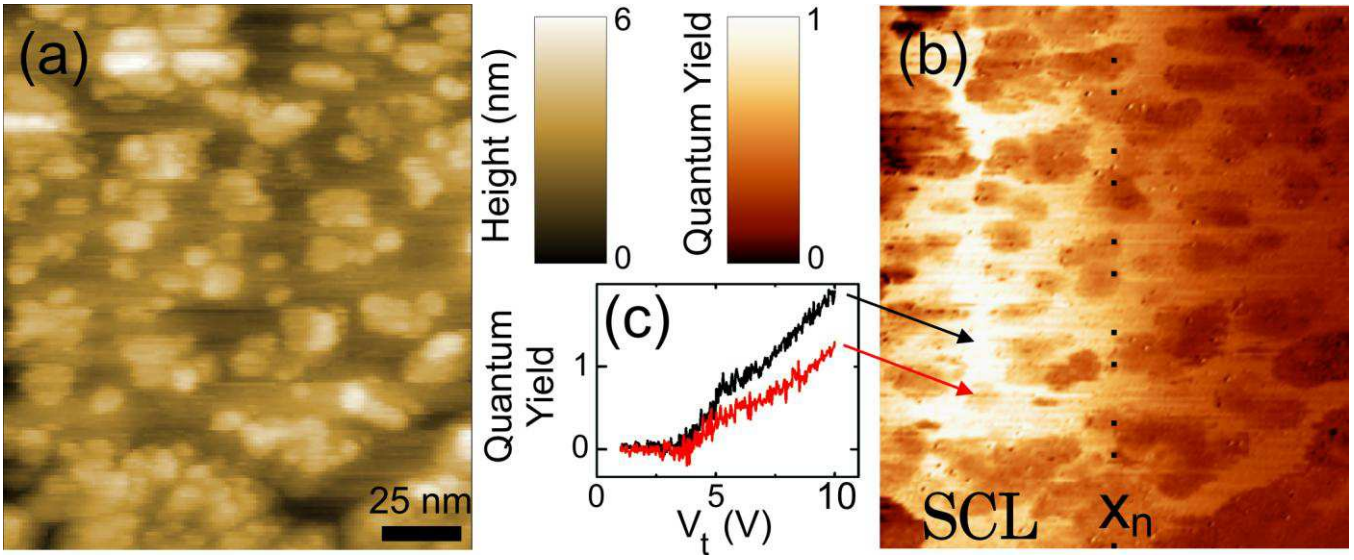
(a)
25 nm
Height (nm)
6
0
Quantum Yield
1
0
(c)
Quantum Yield
1
0
0
5
10
V_t (V)
(b)
SCL
x_n

FIGURE 4

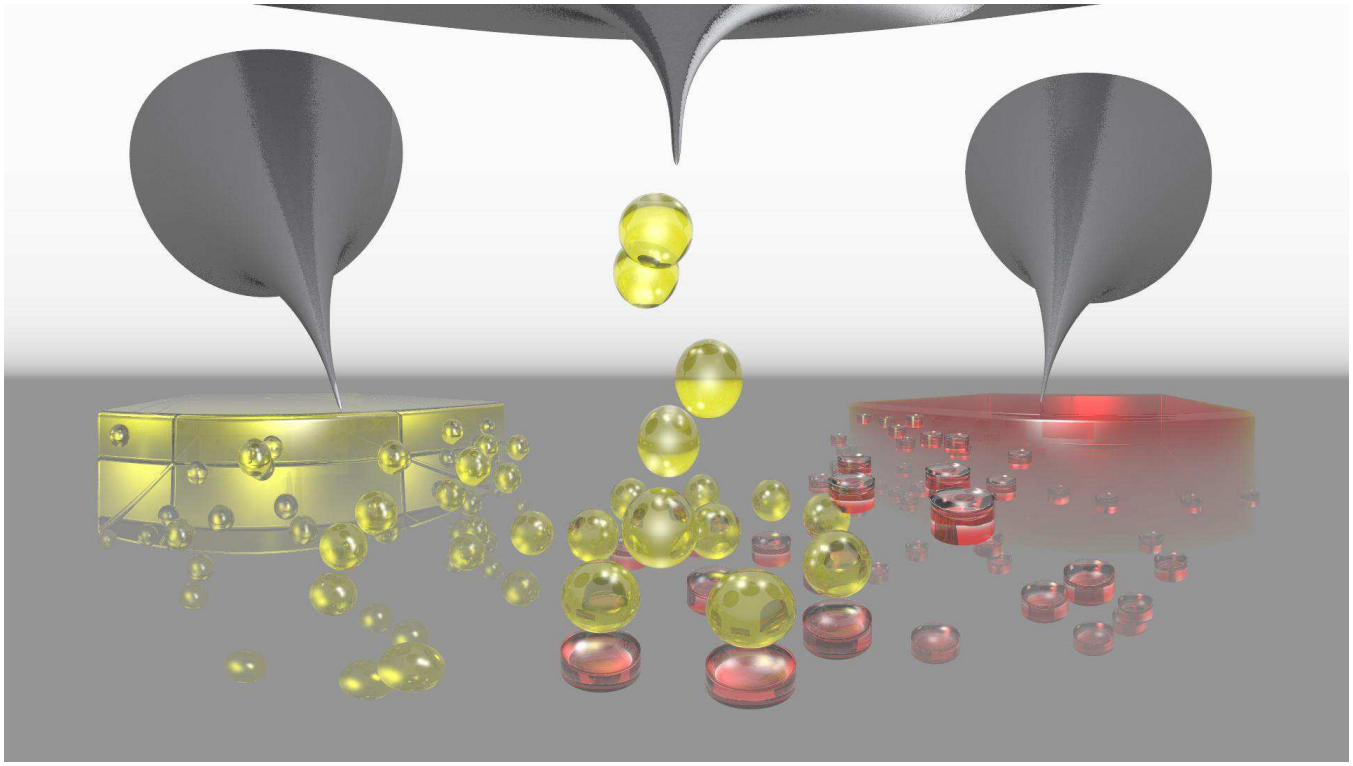

For TOC Only